

pubs.acs.org/joc Article

2-(1,1-Dicyanomethylene)rhodanine-Functionalized Oligothiophenes: A Structure—Property Investigation of *Z/E* Photoisomerization Behavior

Cory T. Kornman, Parag Das, Lei Li, Asmerom O. Weldeab, Ion Ghiviriga, and Ronald K. Castellano*



Cite This: J. Org. Chem. 2024, 89, 13853–13867



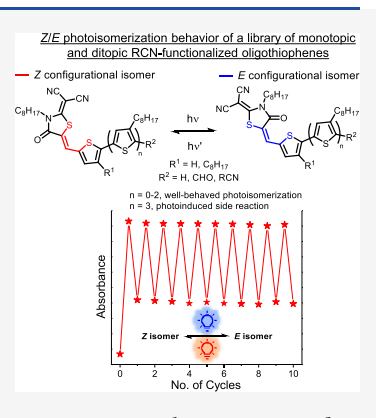
ACCESS I

Metrics & More

Article Recommendations

Supporting Information

ABSTRACT: A series of oligothiophenes singly and doubly functionalized with dicyanorhodanine (RCN) units have been investigated to understand their Z/E photoisomerization behavior upon structural modulation. Monotopic RCN target molecules (1-Z-9-Z) were designed to observe the consequences of π -conjugation, solubilizing group substitution, and formylation of the thiophene units. In all cases, the Z isomer is obtained from synthesis as the thermodynamically stable isomer, whereas the E isomer is achieved through selective irradiation (including red light, $\lambda_{\rm irr}$ = 628 nm) as a Z/E mixture in solution. For the quarterthiophene entries, photoisomerization is inhibited, with photoirradiation resulting only in degradation. The result comports with concentration-dependent studies, which show that increasing π -conjugation results in greater aggregation and muted Z/E photoisomerization. Ditopic RCN targets (10-ZZ-12-ZZ), mimicking acceptor—donor—acceptor (A-D-A) oligomers relevant to OPV materials, also show evidence of photoisomerization in solution, with formation of Z,Z/Z,E mixtures at the photostationary state (PSS). Complementary ground- and excited-state DFT



calculations show excellent agreement with the experimental findings. This comprehensive structure—property analysis is expected to both guide and caution the functional materials community with respect to the usage of photoisomerizable RCN-oligothiophenes for optoelectronic applications.

INTRODUCTION

2-(1,1-Dicyanomethylene)rhodanine (RCN) is an electrondeficient heterocycle derived from the rhodanine core structure (Figure 1a). When the thiocarbonyl is replaced with a dicyanomethylene group, the structure is colloquially referred to as "dicyanorhodanine" and is often abbreviated "RCN" in the organic materials literature (Figure 1b).2 RCN was first reported as an electron acceptor unit for organic materials applications in 2011,³ and has since become popular within the organic materials community. When attached in conjugation with electron-rich donor moieties, RCN can confer many desirable attributes including red-shifted optical absorption, enhanced crystallinities, and significant intramolecular chargetransfer character. Donor-acceptor (D-A) designs featuring RCN have been widely explored in the context of smallmolecule donor and nonfullerene acceptor molecules used for bulk-heterojunction (BHJ) organic photovoltaic (OPV) applications (Figure 1c), 8,9 and many high-performing devices have been reported. 4,10-12

RCN is conjugated with electron-rich donor moieties through an exocyclic double bond that can exist either as the *Z* or *E* stereochemical isomer (Figure 1d–1e). Unanticipated photochemical reactions concerning this exocyclic olefin have been speculated in the past, ¹³ and investigations into the photochemical reactivity have been disclosed for rhodanine derivatives and other electron-deficient units similar to RCN,

as it relates to photovoltaic device performance. 14-16 More recently, the well-behaved Z/E photoisomerization of two simple RCN-functionalized thiophenes was reported for the first time by our lab, sparking questions about how the stereochemistry and photochemical behavior of RCN-functionalized materials might impact the use of this acceptor unit as a component within the BHJ active layer of OPV materials. 17 This was followed by an investigation into RCN-based thinfilms, aimed at defining changes in morphology and optical properties as a function of photochemically obtained isomeric composition.¹⁸ To further highlight the well-behaved photoisomerization of rhodanine and the RCN cores, Dube and coworkers recently reported rhodanine-based chromophores as molecular photoswitches and their application in light-induced apoptosis. 19 Our group also developed a series of RCN-pyrrole conjugates as remarkably efficient bistable photoswitching scaffolds in solution and a polymer matrix.²⁰ Thiophene and benzothiophene heterocycles have also been shown to be key

Received: April 5, 2024
Revised: August 20, 2024
Accepted: September 12, 2024
Published: September 18, 2024





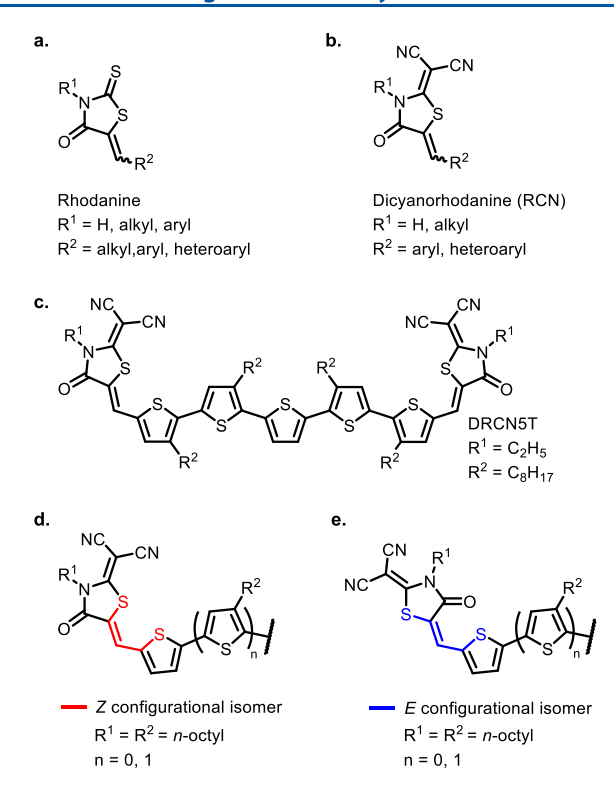


Figure 1. (a) Rhodanine core structure. (b) Dicyanorhodanine core structure. (c) Small molecule donor molecule (DRCNST) functionalized on both termini with RCN acceptor units. RCN-functionalized thiophenes depicted in (d) the Z configuration (red) and (e) the E configuration (blue).

components of highly proficient hemithioindigo (HTI) photoswitches.²¹

Our initial works on the characterization of simple RCN-thiophenes^{17,18} functionalized with mono-, bi-, and terthiophene units (1-Z-3-Z, Figure 2a) prompted us to consider the photochemistry of more complex molecular systems. Here we are interested in the design and synthesis of a library of homologous RCN-functionalized model compounds for a structure-property investigation aimed at differentiating observed photochemical behavior as a function of molecular structure (Figure 2a-d, 1-Z-12-ZZ). Specifically, by increasing the number of conjugated thiophene units functionalized with RCN, investigations into the isomeric distributions at the photostationary state (photostationary state distributions, PSDs) of each model compound are possible as a function of increasing π -conjugation in the donor moiety, more closely resembling the type of structures relevant to the OPV materials community (Figure 2a). We are also interested in the effect of solubilizing group substitution on the thiophene unit directly adjacent to the exocyclic olefin, closely mimicking the structural design of OPV-relevant RCN-functionalized materials (Figure 2b, 5-Z-7-Z).4,11 In addition, electronic modulation at the terminal thiophene unit opposite to the RCN group via electron-withdrawing aldehyde substitution (Figure 2c, 8-Z-9-Z) allows a comparison between formylated and nonformylated RCN-functionalized model compounds. Finally, symmetrical "ditopic" RCN model compounds, featuring RCN substitution on both termini of a thiophene π -system, draw conclusions about the most-common structural designs present in the literature and help understand the photo-

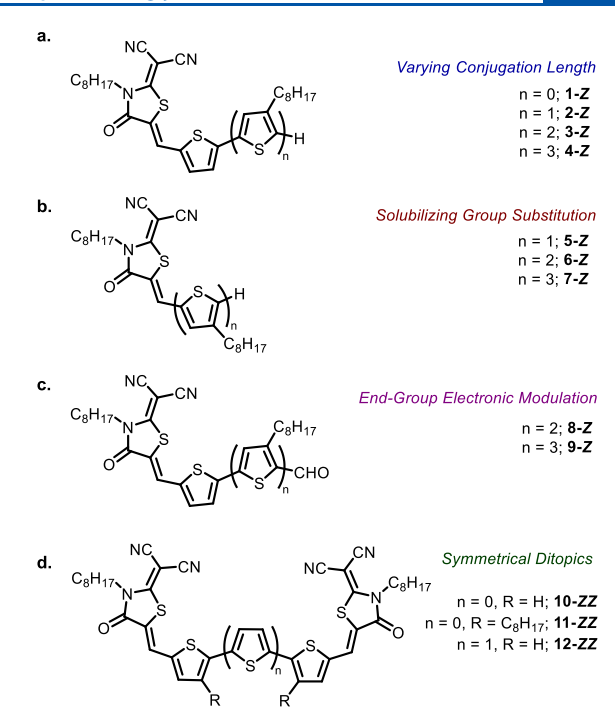


Figure 2. RCN-functionalized oligothiophene targets featuring (a) varying conjugation length, (b) solubilizing group substitution, (c) end-group electronic modulation, and (d) symmetrical ditopic RCN units. (all target molecules are depicted in the *Z* or *Z*,*Z* configuration)

chemical behavior of RCN-molecules bearing two photoactive double bonds (Figure 2d, 10-ZZ-12-ZZ).

Herein, we report the synthesis and photoisomerization of 12 homologous RCN-functionalized model compounds, 1-Z-12-ZZ. We have chosen molecules differing in conjugation length (Figure 2a, 1-Z-4-Z), solubilizing group substitution (Figure 2b, 5-Z-7-Z), electronic modulation (Figure 2c, 8-Z-9-Z), and mono- versus di-RCN functionalization (Figure 2d, 10-ZZ-12-ZZ). The olefin stereochemistry of the assynthesized monofunctionalized RCN targets (1-Z-9-Z) was confirmed as the Z configuration using ¹H NMR, whereas the difunctionalized target molecules were found to have the Z,Z configuration as the thermodynamically stable state, as confirmed using 2D NMR techniques (IPAP-gHSMBC, chloroform-d).

Relative configurational (Z/E) and conformational (s-cis/strans) energetics were investigated using density functional theory (DFT) for the mono- and difunctionalized RCN derivatives, where the lowest energy conformers in the ground state were found to be in accordance with the thermodynamically stable states obtained from synthesis. The photoisomerization behavior of 1-Z-9-Z was investigated by ¹H NMR using multiple wavelengths of LED irradiation (254, 454, 523, and 628 nm) as well as ambient laboratory light, where it was found that all the monofunctionalized RCN derivatives with up to three conjugated thiophene units (1-Z-3-Z, 5-Z-8-Z) are susceptible to the photoisomerization process with the final Z/E PSDs being dependent on the wavelength and intensity of excitation. However, target molecules featuring quarterthiophene π -systems (4-Z and 9-Z) resist the isomerization process almost entirely, resulting in degradation under all wavelengths of selective excitation. The difunctionalized RCN target molecules (10-ZZ-12-ZZ) display well-behaved isomerization behavior under multiple

Scheme 1. Synthesis of Selected (a) Monotopic (3-Z, 4-Z, 8-Z, and 9-Z) and (b) Ditopic (10-ZZ, and 11-ZZ) RCN Oligothiophenes

wavelengths of irradiation (254, 454, 523, and 628 nm) to result in isomeric mixtures of the thermodynamically stable *Z,Z* and metastable *Z,E* forms at the photostationary state (PSS). Interestingly, the *E,E* isomers for 10, 11, or 12 were not observed postirradiation. The photophysical properties of 1-*Z*–12-*ZZ* were explored experimentally (UV–vis, chloroform) and computationally (TD-DFT, gas-phase). Overall, this work provides an in-depth analysis of photochromic RCN-functionalized thiophenes relevant to downstream optoelectronics applications, focusing on structure–property relationships governing their isomerization in solution.

■ RESULTS AND DISCUSSION

Synthesis. The synthetic schemes, written procedures, and detailed characterization data are provided in the Supporting Information (pages S3–S43). Compounds 1-Z-3-Z were synthesized (Schemes S1 and S2a) according to our previous work, ^{17,18} with optimization from the existing literature. ²² Beginning with the synthesis of 4-Z, NBS bromination of terthiophene precursor 17 gives compound 18, which can undergo a final Stille coupling with stannylated thiophene 14 to generate the required quarterthiophene analog 19 bearing aldehyde substitution at the terminal position (Scheme S2b). A condensation reaction between the RCN unit 13 and the formylated quarterthiophene 19 generates the final 4-Z target molecule (Scheme S2b).

The synthetic schemes for 5-Z-9-Z are shown in the Supporting Information (Schemes S2c and S3). The synthesis of 5-Z begins with the formylation of commercially available 3-n-octylthiophene via n-BuLi deprotonation followed by quenching the anion with DMF to yield the formylated

thiophene **20**. A final condensation between RCN **13** and compound **20** yields the **5**-*Z* substrate (Scheme S2c). NBS bromination of 3-*n*-octylthiophene achieves selective halogenation to yield intermediate **21** (Scheme S3a), followed by Vilsmeier—Haack formylation to yield compound **22**. Stille coupling between **22** and **14** yields the formylated bithiophene **23**, which can undergo condensation with RCN to generate target molecule **6**-*Z* (Scheme S3a). Separately, intermediate **23** can be subjected to NBS bromination to generate compound **24**, followed by Stille coupling with **14** to yield intermediate **25**. A condensation reaction between RCN and compound **25** yields **7**-*Z* (Scheme S3b). The formylated target molecules (8-*Z* and 9-*Z*) were prepared by Vilsmeier—Haack formylation of **3**-*Z* and **4**-*Z*, respectively (Scheme **1a**, Scheme S3c,d).

The ditopic RCN-functionalized molecules (10-ZZ-12-ZZ) were prepared using different synthetic approaches (Scheme 1b, Scheme S4).²³ A Pd-catalyzed homocoupling reaction of commercially available 5-bromothiophene-2-carboxaldehyde yields the formylated bithiophene 26, followed by condensation with two molar equivalents of RCN to give compound 10-ZZ. Compound 11-ZZ was prepared in a similar manner, utilizing the same homocoupling starting with compound 22 to yield the bithiophene intermediate 27 (Scheme S4b). The synthesis of 12-ZZ begins with 2,5-dibromothiophene and 5bromothiophene-2-carboxaldehyde which undergo a one-pot, sequential lithium-halogen exchange, followed by a Stille coupling reaction to achieve the diformylated terthiophene intermediate 28. A condensation reaction between the RCN unit 13 (two molar equivalents) and compound 28 yields target molecule 12-ZZ (Scheme S4c).

From the synthetic procedures used for the monotopic RCN-functionalized target molecules (1-Z-9-Z) the Z isomer was the only detectable isomer isolated from the synthesis as confirmed by ¹H NMR, in agreement with our previous work. ¹⁷ For the ditopic RCN-functionalized molecules (10-ZZ-12-ZZ), the Z,Z isomer was the only detectable isomer isolated from the synthesis. This was confirmed by solution 2D-NMR experiments (IPAP-gHSMBC, chloroform-d) performed using 10 as a model compound (Figures S55-S59, vide infra).

Stereochemical Characterization. The as-synthesized isomeric forms of each monofunctionalized RCN target molecule (1-Z-9-Z) were determined to be the Z isomers in all cases, with no observable evidence of the corresponding E isomers visible by thin-layer chromatography (TLC) or crude ¹H NMR analysis of the reaction mixtures. The exocyclic olefin configuration of compound 1-Z was determined in the solidstate by X-ray crystallography and in solution (chloroform-d) by IPAP-gHSMBC as detailed in our previous work. The olefin stereochemistry of compounds 2-Z-9-Z were determined by ¹H NMR (chloroform-d). The chemical shift of the exocyclic olefin proton for monotopic RCN target molecules in the Z configuration is diagnostic and significantly deshielded (ca. 8.00 ppm) compared to the same proton in the Econfiguration (ca. 7.40 ppm) making stereochemical determination by ¹H NMR straightforward. The as-synthesized isomeric forms of the ditopic RCN molecules (10-ZZ-12-ZZ) were determined to be Z_iZ in all cases, with no evidence of the corresponding Z,E or E,E forms resulting from the synthetic procedures used to generate each species.

Using 10-ZZ as a model compound to characterize the olefin stereochemistry of the ditopic RCN substrates, a chemical shift assignment was performed using a combination of ¹H, ¹³C, HSQC, and HMBC experiments (Figures S55-S58, Supporting Information). IPAP-gHSMBC (chloroform-d) analysis of as-synthesized 10-ZZ revealed that the three-bond heteronuclear coupling constant $\binom{1,3}{J_{C18-H11}}$ between the exocyclic olefin proton (H11) and the rhodanine carbonyl carbon atom (C18) was 5.7 Hz (Figure S59a), in agreement with RCNfunctionalized thiophenes and the literature precedent concerning analogous oxazolone heterocycles. 17,24 Upon irradiation of 10-ZZ in solution to a photostationary state (chloroform-d, λ_{irr} = 454 nm, vide infra), the photochemically obtained isomeric mixture was analyzed by NMR (Figures S59b and S72). Solution NMR experiments reveal that irradiation of 10-ZZ results in an isomeric mixture of thermodynamically stable 10-ZZ and metastable 10-ZE forms at the photostationary state (PSS), with no evidence of the 10-EE form present in the mixture (Figure S59b). Solution IPAPgHSMBC analysis of the 10-ZZ/10-ZE mixture reveals that the three-bond heteronuclear coupling constant (1,3 J_{C18-H11}) is much larger for the RCN unit in the E configuration (Z,E isomer, $^{1,3}J_{\text{C18-H11}} = 11.0 \text{ Hz}$) than the Z configuration (Z,Z isomer, $^{1,3}J_{\text{C18-H11}} = 5.7 \text{ Hz}$). The ^{1}H NMR chemical shifts for compounds 11 and 12 show the same trends when comparing the as-synthesized forms (Z,Z) to the photostationary state mixtures (Z,Z/Z,E), confirming that both 11 and 12 were isolated as the Z,Z isomers and irradiation to a PSS generates Z,Z/Z,E mixtures, with no evidence of the E,E form in any case (Figure 6, Figures S73-S74, vide infra).

NMR Photoisomerization Studies. The photoisomerization reactions of RCN-functionalized target molecules 1-Z-12-ZZ are conveniently monitored by solution ¹H NMR

(chloroform-*d*) by comparing the spectrum of the assynthesized isomer with the spectrum of the same sample postirradiation. Full details of the selective irradiation sources used for the photoisomerization studies can be found in the Supporting Information (Pages S46–S47, Figure S60). The distribution of thermodynamically stable forms (*Z* or *Z*,*Z* isomers) and metastable forms (*E* or *Z*,*E* isomers) at the PSS is quantified as the photostationary state distribution (PSD) and the PSDs determined from the ¹H NMR integration ratios in case of all the model compounds (1-*Z*-12-*ZZ*) under varying wavelengths are summarized in Table 1. The ¹H NMR spectra summarizing the photoisomerization results of each RCN-functionalized target molecule can be found in the Supporting Information (Figures S63–S88).

Table 1. Solution ¹H NMR-Determined Isomeric Photostationary State Distributions Achieved by Irradiation to a Photostationary State in Chloroform-*d* at a 15 mM Concentration Unless Otherwise Specified

	PSD (Z/E or $Z,Z/Z,E$) @ λ_{irr}					
target molecule	254 nm ^a	454 nm ^b	523 nm ^b	628 nm ^b	ambient ^{b,c}	
1- Z	56/44	98/2 ^d	100/0	100/0	89/11	
2 -Z	69/31	51/49	83/17	97/3	79/21	
3- Z	66/34 ^d	66/34	73/27	87/13	74/26	
4- Z	86/14 ^d	93/7 ^d	99/1 ^d	93/7 ^d	89/11	
5- Z	53/47	99/1 ^d	100/0	100/0	80/20	
6- Z	65/35	53/47	81/19	100/0	76/24	
7-Z	99/1 ^d	69/31	73/27	88/12	74/26	
8- Z	88/12 ^d	80/20	82/18	93/7	78/22	
9- Z	95/5 ^d	95/5 ^d	$93/7^{d}$	99/1 ^d	91/9	
10- ZZ	100/0	75/25	85/15	93/7	85/15	
11- ZZ	96/4	82/18	87/13	96/4	88/12	
12- ZZ	99/1 ^d	92/8	91/9	93/7	94/6	

^aPhotostationary state distributions (PSDs) are reported as the average of four separate measurements (standard error <1%). ^bPhotostationary state distributions (PSDs) are reported as a single measurement. ^cAmbient irradiation experiments were performed using solutions at 7.5 mM concentration. ^dIrradiation resulted in various photoproducts and photodegradation not consistent with Z/E photoisomerization.

Monotopic RCN target molecules bearing one- to threethiophene units (1-Z-3-Z) and (5-Z-8-Z) display well-behaved isomerization reactions under multiple wavelengths of selective irradiation (λ_{irr} = 254, 454, 523, and 628 nm) and under ambient irradiation conditions, whereas monotopic RCN substrates functionalized with quarterthiophene π -systems (4-Z and 9-Z) show only minor evidence of $Z \rightarrow E$ photoisomerization accompanied by photodegradation and/ or formation of other photoproducts not consistent with olefin isomerization reactions, except in the case of ambient irradiation conditions. All ditopic RCN model compounds (10-ZZ-12-ZZ) undergo well-behaved Z/E photoisomerization reactions under multiple wavelengths of selective irradiation (254, 454, 523, and 628 nm) to result in isomeric distributions composed of Z,Z and Z,E forms at the PSS, with no evidence of the E,E forms under prolonged irradiation conditions.

To understand the effects of solubilizing group substitution on the observed PSD, compounds 5-Z-7-Z were assessed in comparison with compounds 1-Z-3-Z. For compound 1-Z, the ¹H NMR aromatic signals representing the as-synthesized

isomer appear to duplicate upon irradiation with ultraviolet (UV) light (chloroform-d, $\lambda_{\rm irr}=254$ nm) resulting in a 56/44 (Z/E) isomeric mixture at the PSS (Figure 3a). The effect of n-octyl substitution on the thiophene directly adjacent to the RCN acceptor unit results in a small, but observable difference in the experimental PSD.

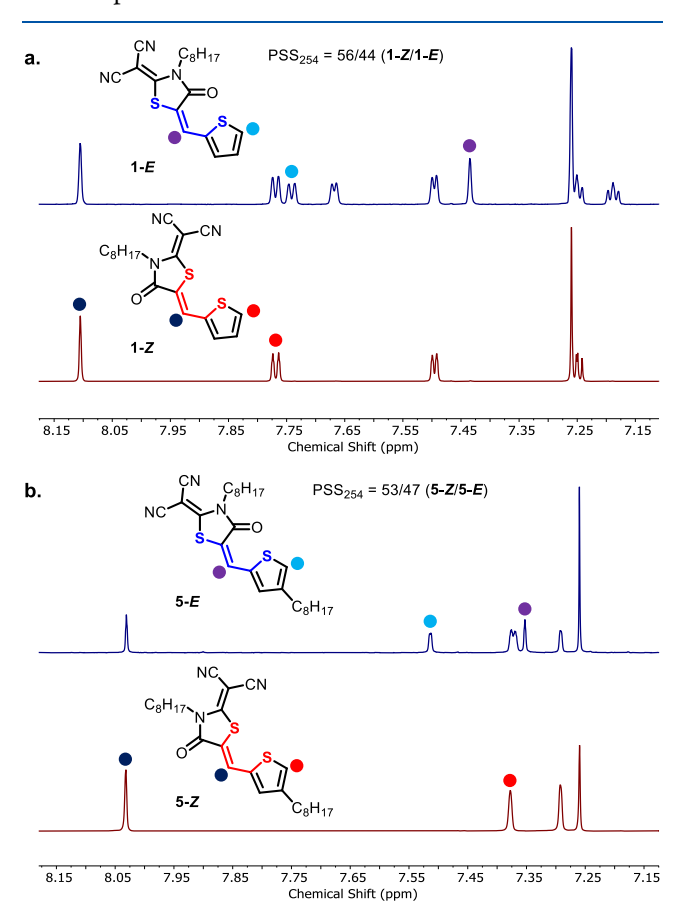


Figure 3. 1 H NMR spectra (chloroform-d) showing (a) pure 1-Z (bottom) and 1-Z/E mixture (top) resulting from 254 nm irradiation; (b) pure 5-Z (bottom) and 5-Z/E mixture (top) resulting from 254 nm irradiation.

Under UV illumination ($\lambda_{irr} = 254$ nm) compound 5-Z underwent a 3% increase in $Z \rightarrow E$ conversion compared to compound 1-Z, resulting in a mixture of 53% 5-Z and 47% 5-E in chloroform-d at the PSS (Figure 3b). Interestingly, switching to a longer wavelength of irradiation (blue LED, $\lambda_{\rm irr}$ = 454 nm) results in only minor evidence of Z/Eisomerization for both 1-Z and 5-Z, accompanied by formation of various photoproducts not consistent with $Z \rightarrow E$ isomerization (Figures S63, S67, and S87). This is an interesting result considering that the primary charge transfer band observed by UV-vis (λ_{max} , chloroform, 20 μ M) absorbs most strongly between ca. 350-460 nm for 1-Z and 5-Z, respectively (Figure S89), with 454 nm illumination overlapping primarily with the onset of absorption observed for both species. Not surprisingly, irradiation at longer wavelengths of light (λ_{irr} = 523 and 628 nm) produces no observable photochemistry for 1-Z and 5-Z as neither of these species absorb past 460 nm in chloroform (Figures S63 and S67). Similar to the trend observed for ultraviolet irradiation, ambient (laboratory) irradiation conditions result in greater Z \rightarrow E conversion for 5-Z compared to 1-Z, resulting in PSDs of 80/20 (Z/E) and 89/11 Z/E for 5-Z and 1-Z, respectively (Figures S75 and S79, Table 1).

The photoisomerization reactions (in chloroform-d) of 2-Z and 6-Z bearing two thiophene units were compared under varying wavelengths of irradiation (Table 1). UV irradiation of compound 2-Z in chloroform-d results in a 69/31 (Z/E) distribution at the PSS, with no evidence of photodegradation under these irradiation conditions (Figure S64, Table 1). The same irradiation conditions applied to compound 6-Z resulted in a PSD of 65/35 (Z/E), demonstrating a 4% increase in $Z \rightarrow$ E conversion for the dioctyl-substituted bithiophene derivative (6-Z) compared with compound 2 (Figure S68). Similarly, with blue and green LED (Figures S64 and S68) irradiation, a minor but notable change in isomeric Z/E composition was observed for compounds 2-Z and 6-Z (Table 1), with both resulting in well-behaved Z/E isomerization reactions with no evidence of other photochemical events. Not surprisingly, red LED irradiation resulted in only minor evidence of Z/Eisomerization for compounds 2 and 6 (Table 1), given that neither molecule absorbs strongly in this range. Samples of 2-Z and 6-Z exposed to ambient (laboratory) light conditions were susceptible to photoisomerization reactions, resulting in PSDs of 79/21 (2-Z/2-E) and 76/24 (6-Z/6-E) for compounds 2 and 6, respectively (Figures S76 and S80, Table 1).

With absorbance spectra extending beyond the range of 630 nm upon increased conjugation (Figure 7 and Figure S89), compounds 3-Z and 7-Z represent some of the most well-behaved photoswitching RCN-functionalized molecules, with both species undergoing isomerization reactions under illumination across the visible spectrum ($\lambda_{\rm irr}=454-628$ nm). While some amount of photodegradation was observed under UV irradiation for 3-Z and 7-Z, photostationary state distributions ranging between 88/12 (Z/E) and 66/34 (Z/E) were observed under visible (LED) irradiation conditions (Figures S65 and S69, Table 1). Under UV irradiation, compound 3-Z underwent significant $Z \rightarrow E$ conversion, resulting in a 66/34 (3-Z/3-E) mixture at the PSS, accompanied by evident photodegradation.

Interestingly, although similar in structure and optical absorbance properties, compound 7-Z resisted the olefin isomerization process almost entirely under 254 nm irradiation conditions, resulting in primarily degradation events under UV light (Figure S69, Table 1). However, upon blue, green, and red LED irradiation, both compounds 3 and 7 displayed reactivity solely attributed to Z/E isomerization, resulting in minorly different but notable Z/E isomeric ratios at the PSS, when compared at the same irradiation conditions (Figure 4, Table 1). The well-behaved photoisomerization using red LED can be interesting for photoresponsive functional materials development upon further structural modification of these oligothiophenes.

Comparing aldehyde-functionalized RCN target molecules (8-Z and 9-Z) with corresponding analogs lacking the same electron-withdrawing modulation (3-Z and 4-Z), a decrease in the $Z \rightarrow E$ conversion was observed for the aldehyde-functionalized molecules. RCN-functionalized molecules with terthiophene systems (3-Z and 8-Z) and quarterthiophene π -systems (4-Z and 9-Z) all displayed evidence of photoisomerization under 254 nm irradiation, resulting in Z/E mixtures of 66/34, 86/14, 88/12, and 95/5 for 3-Z, 4-Z, 8-Z, and 9-Z, respectively, accompanied by significant evidence of photodegradation for each sample (Figures S65—S66, S70, and S71). However, with selective excitation in the visible region

8.10 8.00

7.90 7.80 7.70

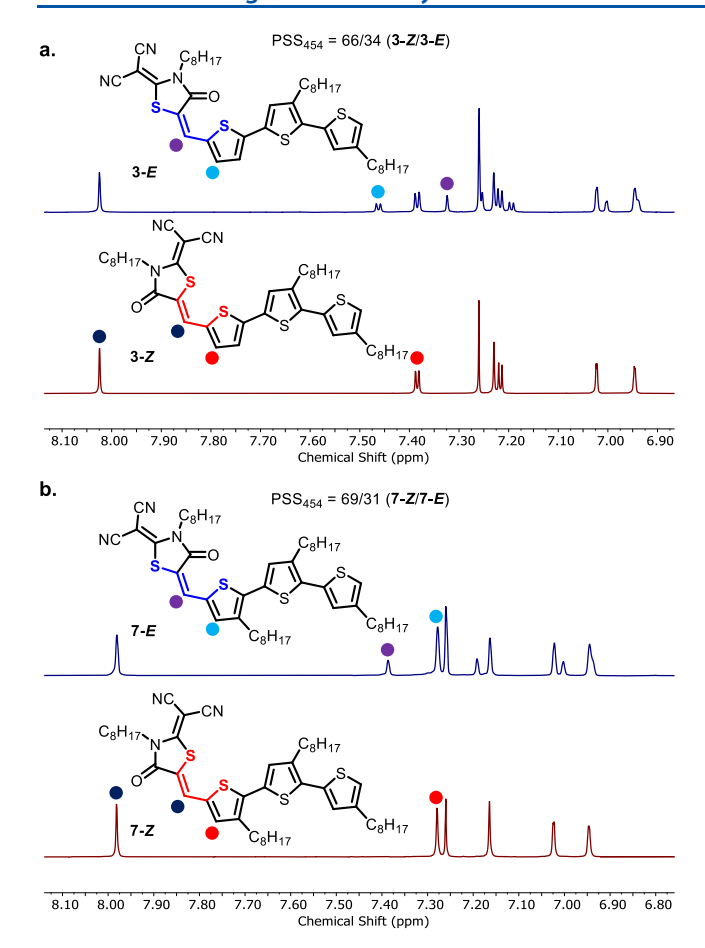


Figure 4. ¹H NMR spectra (chloroform-d) showing (a) pure 3-Z (bottom) and 3-Z/E mixture (top) resulting from 454 nm irradiation; (b) pure 7-Z (bottom) and 7-Z/E mixture (top) resulting from 454 nm irradiation.

(LED light sources) as well as broad-spectrum ambient irradiation, well-behaved isomerization reactions were observed for the terthiophene derivatives (Table 1). Comparing the Z/E PSDs, a decrease in $Z \rightarrow E$ conversion was observed for aldehyde-substituted compound 8 versus nonformylated analog 3, under the blue (14%), green (9%), and red (6%) LED, and ambient (4%) irradiation conditions (Table 1).

Interestingly, by adding an extra thiophene unit, thus moving from terthiophene (3-Z, 7-Z, and 8-Z) to quarterthiophene (4-Z and 9-Z), the previously observed isomerization behavior is largely suppressed (Figure S88). While the terthiophene systems display predictable isomerization reactions under the full visible spectrum, the quarterthiophene target molecules resulted in primarily photodegradation under all selective wavelengths of irradiation ($\lambda_{irr} = 254-628$ nm) with only minor evidence of Z/E photoisomerization (Table 1). The best isomerization results for 4-Z and 9-Z were obtained under ambient irradiation conditions (Figure 5), where compound 4-Z resulted in a PSD of 89/11 (4-Z/4-E) compared to the 91/9 (9-Z/9-E) mixture observed for the aldehyde-functionalized quarterthiophene analog 9-Z (Figure 5, Table 1). While for INCN-functionalized donor—acceptor molecules, another popular class of OPV materials, the photodegradation pathways are well-demonstrated, 27-30 ploring the photodegradation behavior of the RCN-oligothiophenes would be insightful for the OPV community to leverage more robust designs of functional organic materials.

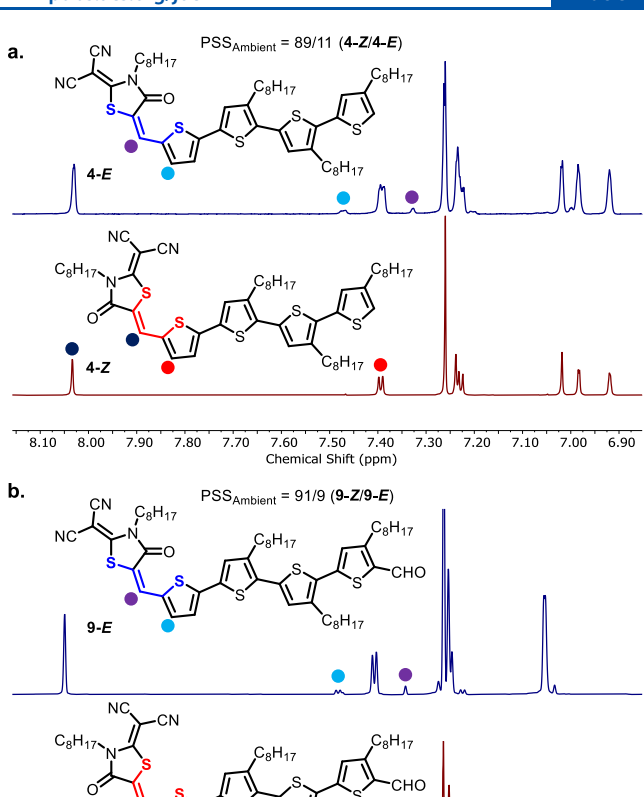


Figure 5. ¹H NMR spectra (chloroform-*d*) showing (a) Pure 4-*Z* (bottom) and 4-*Z/E* mixture (top) resulting from ambient irradiation. (b) Pure 9-*Z* (bottom) and 9-*Z/E* mixture (top) resulting from ambient irradiation.

Chemical Shift (ppm)

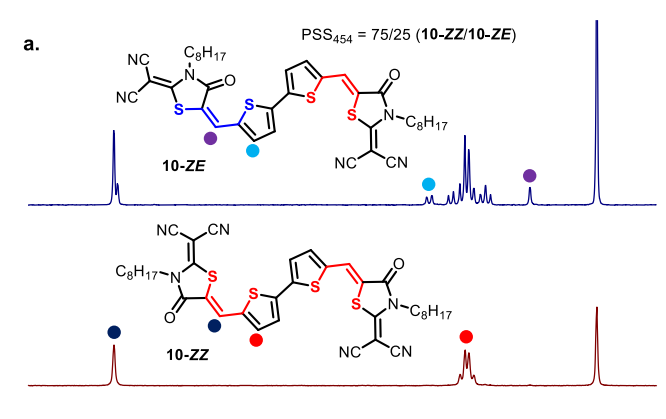
7.60 7.50

7.40

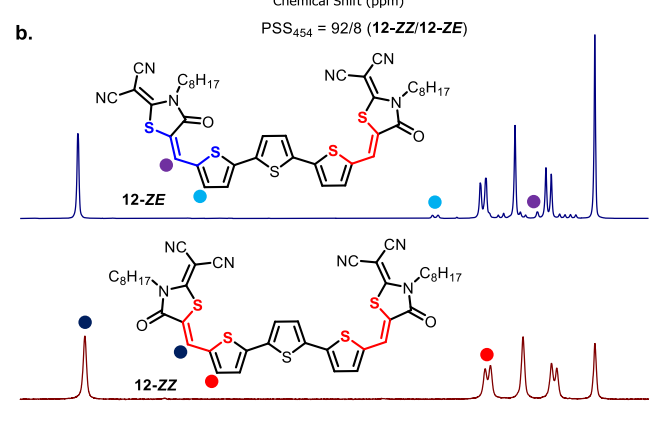
7.30 7.20

7.10

The ditopic RCN-functionalized molecules (10-ZZ-12-ZZ) demonstrate well-behaved isomerization reactions under all selective excitation wavelengths in the visible region (454, 523, and 628 nm). Upon irradiation to a PSS, the ditopic RCNfunctionalized model compounds display mixtures of thermodynamically stable Z,Z and metastable Z,E forms, with no evidence of the E,E isomer in any case. Under 454 nm irradiation, compound 10-ZZ undergoes isomerization to generate a 75/25 (10-ZZ/10-ZE) mixture at the photostationary state (Figure 6a, Table 1). Green and red LED irradiation of 10-ZZ in chloroform-d also promotes Z/Eisomerization reactions, resulting in PSDs of 85/15 (Z,Z/Z,E) and 93/7 (Z,Z/Z,E) from 523 and 628 nm irradiation sources, respectively (Figure S72, Table 1). Compound 11-ZZ displays well-behaved isomerization under all wavelengths of selective irradiation, resulting in PSDs of 96/4, 82/18, 87/13, and 96/4 (11-ZZ/11-ZE) for 254, 454, 523, and 628 nm excitation wavelengths, respectively (Figure S73, Table 1). Irradiation of compound 12-ZZ in chloroform mostly results in degradation under UV light, however, Z/E isomerization was observed upon 454, 523, and 628 nm irradiation to result in isomeric mixtures of 92/8, 91/9, and 93/7 (12-ZZ/12-ZE), respectively (Figure S74, Table 1). Ambient irradiation also results in Z/Ephotoisomerization of the ditopic RCN-oligothiophenes (10-ZZ-12-ZZ) with up to 15% isomerization achieved under these conditions (Figures S84–S86, Table 1).



8.15 8.10 8.05 8.00 7.95 7.90 7.85 7.80 7.75 7.70 7.65 7.60 7.55 7.50 7.45 7.40 7.35 7.30 7.25 7.20 Chemical Shift (ppm)



8.10 8.05 8.00 7.95 7.90 7.85 7.80 7.75 7.70 7.65 7.60 7.55 7.50 7.45 7.40 7.35 7.30 7.25 7.20 Chemical Shift (ppm)

Figure 6. ¹H NMR spectra (chloroform-d) showing (a) pure 10-ZZ (bottom) and 10-ZZ/ZE mixture (top) resulting from ambient irradiation; (b) pure 12-ZZ (bottom) and 12-ZZ/ZE mixture (top) resulting from 454 nm irradiation.

UV-Vis Photoisomerization Studies. Ultraviolet-visible spectroscopy (UV-vis) was used to study the photoisomerization reactions of RCN-functionalized substrates 1-Z-3-Z, 5-Z-8-Z, and 10-ZZ-12-ZZ by monitoring changes to absorption profile of the original (as-synthesized) material as a function of irradiation time (Figures S89–S95, vide infra). The photophysical properties obtained via irradiation to a PSS (chloroform, 20 μ M) and time-dependent DFT-predicted photophysical properties for thermodynamically stable forms (Z or Z,Z) and metastable forms (E or Z,E) are summarized in Table 2. The solution absorption maxima (λ_{max}) for all RCNfunctionalized substrates are attributed to HOMO-LUMO transitions with intramolecular charge-transfer character. The secondary excitations are HOMO-1 to LUMO transitions of π – π * character, as observed by visual inspection of the frontier MOs predicted by DFT analysis.

The $\lambda_{\rm max}$ transitions for compounds 1-Z and 5-Z lie at 399 and 420 nm, respectively, and the secondary transitions near 300 nm are $\pi-\pi^*$ transitions (Figure S89). Upon irradiation to a photostationary state ($\lambda_{\rm irr}=254$ nm), a 4.2% increase in the $\lambda_{\rm max}$ absorbance was observed for 1-Z, accompanied by a 14 nm redshift in the absorption maximum from the assynthesized target molecule (1-Z, $\lambda_{\rm max}=399$ nm) to the isomeric mixture (1-Z/1-E, $\lambda_{\rm max}=413$ nm) at the PSS (Figure S89a, Table 2). Similar trends were observed upon 254 nm irradiation of 5-Z in chloroform (Figure S89b). A 3.6% increase in maximum absorbance was observed upon

Table 2. Experimental (UV-Vis, Chloroform) and Time-Dependent DFT Simulated (CAM-B3LYP/cc-pVDZ, Gas-Phase) Photophysical Properties for Compounds 1-12

	λ_{\max}^{a} (nm)		$\lambda_{\max}^{b} (nm)/\varepsilon^{c}$		
model compound	Z or Z , Z ^{d}	Z/E or $Z,Z/Z,E^e$	Z or Z,Z	E or Z,E	
1- Z	399	413 ^f	349/34 600	360/37 300	
2 -Z	476	483 ^g	413/43 200	422/49 200	
3- Z	510	517 ^g	449/57 800	458/64 000	
4- Z	525		475/66 900	481/76 600	
5- Z	420	422 ^f	352/35 700	364/38 000	
6- Z	472	481 ^g	412/41 200	424/47 300	
7-Z	506	513 ^g	453/55 000	461/61 300	
8- Z	500	508 ^g	460/65 400	467/72 200	
9- Z	518		482/80 700	488/87 800	
10-ZZ	510	517 ^g	469/74 600	476/80 500	
11- <i>ZZ</i>	446	449 ^g	441/67 500	449/73 200	
12- ZZ	533	537 ^g	491/79 500	496/88 200	

"UV—vis measured as 20 mM solutions in chloroform. ^bDerived from gas-phase time-dependent density functional theory (TD-DFT) at the CAM-B3LYP/cc-pVDZ level of theory. ^cMolar extinction coefficients (ε) reported in L mol⁻¹ cm⁻¹. ^dPhotophysical properties of assynthesized monotopic (Z isomer) and ditopic (Z,Z isomer) substrates. ^eProperties of as-synthesized/metastable isomeric mixtures for monotopic (Z/E) and ditopic (Z,Z/Z,E) substrates obtained via irradiation to a PSS. ^fλ_{irr} = 254 nm. ^gλ_{irr} = 454 nm.

irradiation of 5-Z in solution (λ_{irr} = 254 nm), accompanied by a 2 nm redshift from the pure sample (5-Z, λ_{max} = 420 nm) to the PSS mixture (5-Z/5-E, λ_{max} = 422 nm) achieved postirradiation (Figure S89b, Table 2).

Since the pure samples of 1-E or 5-E could not be isolated, ¹⁷ the theoretical absorption profiles of 1-E and 5-E were simulated using time-dependent density functional theory (TD-DFT) methods. Excited-state calculations were performed at the CAM-B3LYP/cc-pVDZ level for the RCN model compounds after gas-phase geometry optimizations at the B3LYP/6-31+G(d) level of theory. All octyl chains were truncated to methyl groups to reduce the computational cost. For compound 1-Z, the absorbance maximum (λ_{max}) was predicted by TD-DFT to be 349 nm in the gas-phase (Figure S89c). The calculated absorbance profile for 1-E ($\lambda_{\text{max}} = 360$ nm) represents an 11 nm redshift compared to the 1-Z form, accompanied by a 7.7% increase in molar absorptivity (ε) from 1-Z ($\varepsilon = 3.46 \times 10^4 \text{ L mol}^{-1} \text{ cm}^{-1}$) to 1-E ($\varepsilon = 3.73 \times 10^4 \text{ L}$ mol⁻¹ cm⁻¹) as predicted by excited-state DFT calculations (Figure S89c, Table 2). The TD-DFT calculated absorption maxima are 352 and 364 nm for 5-Z and 5-E, respectively. The experimental trends compare very well with the trends observed from the simulated UV-vis spectra, showing a large spectral overlap between Z and E isomers for compounds 1 and 5 (TD-DFT) and Z isomers and Z/E mixtures as obtained postirradiation in chloroform (Figure 7 and S89).

For the monotopic bithiophene derivatives, compounds 2-Z and 6-Z, the HOMO–LUMO charge-transfer bands ($\lambda_{\rm max}$) are at 476 and 472 nm, respectively, with $\pi-\pi^*$ transitions between 300–350 nm for 2-Z (Figure S88a) and 6-Z (Figure 7 and S90b) in chloroform. Irradiation of the 2-Z UV–vis sample (chloroform, 20 μ M) to various photostationary states under 523, 454, and 254 nm excitation are shown in Figure S90a, with the PSS composition at 454 nm hosting the largest concentration of 2-E isomers in solution, in excellent agreement with the 1 H NMR calculated PSDs (Table 1, *vide*

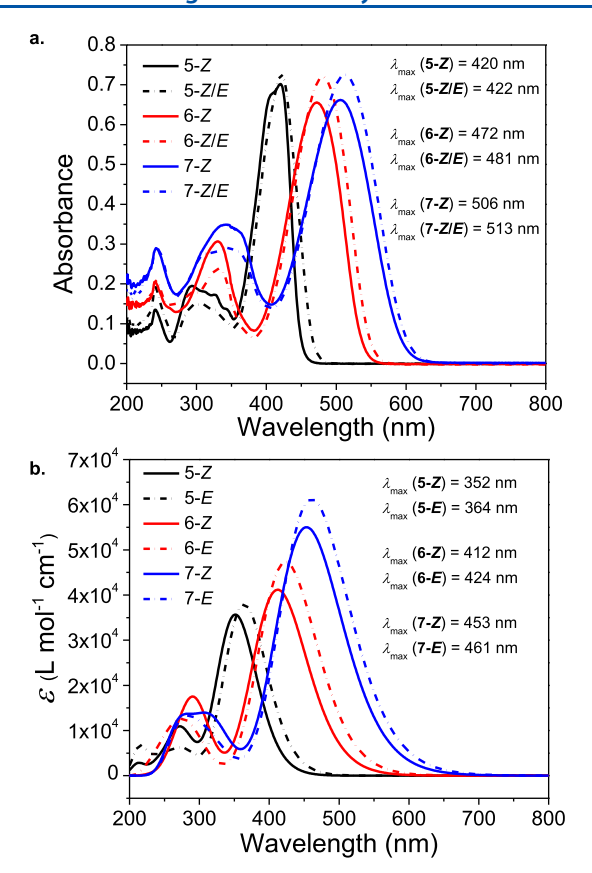


Figure 7. (a) Solution UV—vis absorption spectra (chloroform, 20 μ M) of 5-Z, 6-Z, and 7-Z (solid lines) and corresponding Z/E mixtures obtained after irradiation to a photostationary state (dashed lines). (b) Time-dependent DFT absorption profiles for Z isomers (solid) and E isomers (dashed) of **5**, **6**, and **7**.

supra). The optical profile observed for the 2-Z/E PSS mixture ($\lambda_{\rm max} = 483$ nm) after 454 nm irradiation represents a 7 nm redshift in absorbance maximum compared to the pure sample (2-Z, $\lambda_{\rm max} = 476$ nm), accompanied by a 9.4% increase in absorbance value for the 2-Z/E mixture at the photostationary state ($\lambda_{\rm irr} = 454$ nm).

Compound 6-Z follows the same trends after 523, 454, and 254 nm irradiation (Figure S90b), matching well the relative 6-Z/E isomeric ratios observed for postirradiated samples by ¹H NMR in chloroform-d (Table 1), with the highest extent of Z \rightarrow *E* conversion obtained upon 454 nm irradiation. In addition to the 9 nm redshift, a 9.8% increase in absorbance maximum was observed for the 6-Z/E mixture compared to the $\lambda_{\rm max}$ transition of the pure Z isomer. The computationally derived absorption profiles for compounds 2-Z and 6-Z show λ_{\max} values of 413 and 412 nm, respectively (Figure S90), with the E isomers showing a red-shifted absorption profile for both compounds 2 (9 nm) and 6 (12 nm). Compared to the corresponding Z forms, an increase in the molar absorptivity (ε) for the E isomers was observed for both cases, which confirms the striking resemblance of the computationally derived trends to the solution UV-vis profiles (Figure S90, Table 2).

With compounds 3 and 7, the lowest energy absorption maxima (λ_{max}) were red-shifted compared to previously discussed compounds (1, 2, 5, and 6), due to the larger extent of π -conjugation, and were observed at 510 nm (3-Z) and 506 nm (7-Z), respectively, with π - π * transitions

absorbing most strongly between 290-380 nm for each species in chloroform (Figures S91 and 7). Results from irradiation of 3-Z and 7-Z in chloroform with 628, 523, and 454 nm excitation are shown in the Supporting Information (Figure S91), with the PSS Z/E mixture at 454 nm excitation representing the largest Z to E conversion for both the compounds. The results are further supported by the ¹H NMR calculated PSDs under various irradiation wavelengths (Table 1, vide supra). The UV-vis profiles for the Z/E mixtures of 3 and 7 show a redshift in λ_{\max} compared to the as-synthesized Zisomer, accompanied by an increase in absorbance for the Z/Emixture at the PSS compared to the UV-vis profile of pure Z isomer. The TD-DFT calculated absorption profiles for compounds 3 and 7 show an excellent resemblance to the solution ones and the trend of Z and E isomer profiles matches well with the other target molecules, as detailed in Table 2 and Figure S91.

The $\lambda_{\rm max}$ transition for aldehyde-bearing compound 8-Z absorbs most strongly at 500 nm in chloroform (Figure S93a), which is a 10 nm blue-shift compared to its nonformylated analog 3-Z. Similar photoisomerization behavior was observed for 8-Z, with a gradual increase in absorbance upon $Z \to E$ conversion, accompanied by a redshift in $\lambda_{\rm max}$ as the pure sample is irradiated with 454, 523, and 628 nm light sources to form 8-Z/E mixtures at each respective photostationary state (Figure S93). A $\lambda_{\rm max}$ of 467 nm was observed for the calculated (TD-DFT) absorbance for 8-E, representing a 7 nm redshift with respect to the 8-Z molecule ($\lambda_{\rm max}$ = 460 nm); the trend matches well with the solution results (Figure S93c).

The quarterthiophene analogs 4-Z and 9-Z have the most red-shifted absorption profiles among the monotopic RCN-oligothiohenes, with maximum absorbances observed at 525 and 518 nm, respectively (Figure S92). This can be attributed to the significant π -conjugation present in these molecules. Since photodegradation was observed for 4-Z and 9-Z under selective irradiation NMR experiments, detailed photoisomerization studies by UV-vis were not performed for these compounds. However, TD-DFT simulated absorption profiles for compounds 4 and 9 were calculated and found to show similar trends as the monotopic target molecules (Figure S92, Table 2).

The optical profiles for the ditopic RCN-functionalized model compounds are shown in Figure 8 and in the Supporting Information (Figures S93 and S94). The absorbance maximum for compound 10-ZZ lies at 510 nm in chloroform (Figure 8a). Irradiation of 10-ZZ generates a 10-ZZ/10-ZE mixture at the PSS, which was highest in 10-ZE isomer concentration upon blue LED irradiation ($\lambda_{irr} = 454$ nm). The 10-ZZ/ZE mixture has a λ_{max} value of 517 nm, redshifted from the pure 10-ZZ molecule by 7 nm and accompanied by a 0.5% increase in absorbance for the ZZ/ ZE mixture (Figure 8a). The TD-DFT calculated UV-vis profile for 10-ZZ predicts a λ_{max} value of 469 nm (Figure 8b). A 7 nm redshift was predicted for 10-ZE ($\lambda_{max} = 476$ nm) compared to 10-ZZ (λ_{max} = 469 nm), accompanied by a 7.9% increase in molar absorptivity from 10-ZZ ($\varepsilon = 7.46 \times 10^4 \text{ L}$ $\text{mol}^{-1} \text{ cm}^{-1}$) to 10-ZE ($\varepsilon = 8.05 \times 10^4 \text{ L mol}^{-1} \text{ cm}^{-1}$).

The absorbance maximum for compound 11-ZZ lies at 446 nm in chloroform (Figure 8a), which represents a 64 nm blue-shift from 10-ZZ and can be attributed to the incorporation of octyl chains in the thiophene units. This observation is consistent with introduced steric interactions in the π -conjugated framework resulting in a hypsochromic shift in

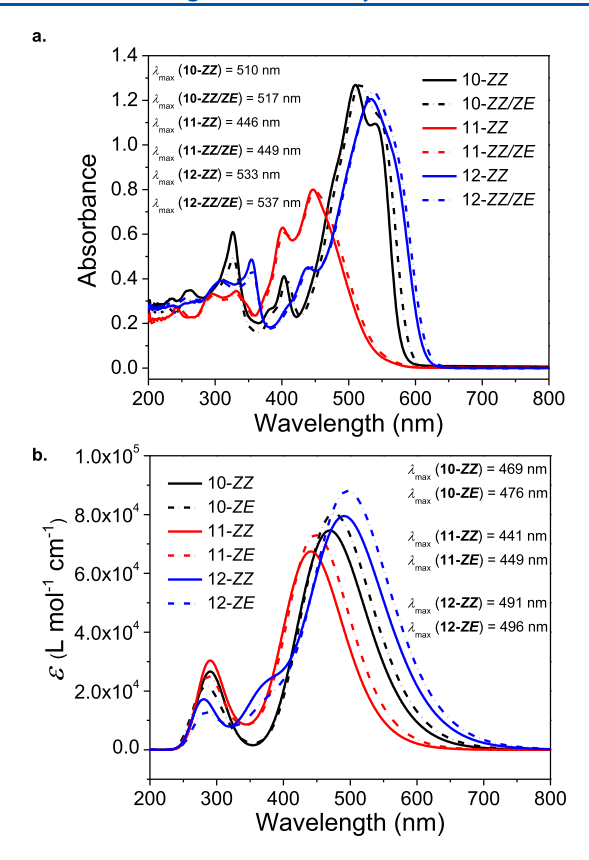


Figure 8. (a) Solution UV–vis absorption spectra (chloroform, 20 μ M) of 10-ZZ, 11-ZZ, and 12-ZZ (solid lines) and corresponding Z,Z/Z,E mixtures obtained after irradiation to a photostationary state (dashed lines). (b) Time-dependent DFT absorption profiles for Z,Z isomers (solid) and Z,E isomers (dashed) of 10, 11, and 12.

the absorption profile. Tonly slight changes were observed in the absorbance profile from the pure sample when irradiated with 523 nm, 454 nm, and 254 nm light to form 11-ZZ/ZE mixtures postirradiation (Figure S93b). Blue LED ($\lambda_{\rm irr}=454$ nm) irradiation initiates the greatest $Z\to E$ conversion based on ¹H NMR studies (Table 1, vide supra), resulting in a 3 nm redshift in $\lambda_{\rm max}$ for the 11-ZZ/ZE mixture ($\lambda_{\rm max}=449$ nm) compared to the pure Z,Z isomer ($\lambda_{\rm max}=446$ nm). Gas-phase DFT simulations predict a $\lambda_{\rm max}$ of 449 nm for 11-ZE, reflecting an 8 nm redshift with respect to the 11-ZZ molecule ($\lambda_{\rm max}=441$ nm), with an 8.5% increase in molar absorptivity (ϵ) between 11-ZE and 11-ZZ (Figure 8b). However, comparable increases in absorbance were not observed upon $Z\to E$ photoisomerization for 11-ZZ and 11-ZZ/ZE (Figure 8a).

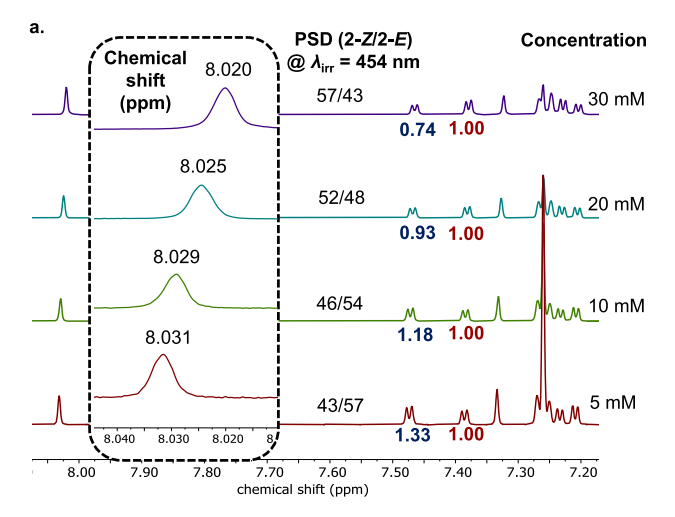
Compound 12-ZZ shows the most red-shifted absorption profile, with a $\lambda_{\rm max}$ of 537 nm, among the three ditopic RCN structures we have investigated, as it offers the most π -conjugation. Upon 454 nm irradiation, a 4 nm redshift was observed for the 12-ZZ/12-ZE mixture at the PSS from the pure 12-ZZ, accompanied by a 2.6% absorbance increase for 12-ZZ/ZE compared to 12-ZZ (Figure 8a and Figure S94). The TD-DFT calculated UV—vis profiles for 12-ZZ and 12-ZE predict $\lambda_{\rm max}$ values at 491 and 496 nm, respectively, accompanied by a 10.9% molar absorptivity increase from 12-ZZ to 12-ZE (Table 2, Figure 8b). Though the *E,E* isomers were not observed experimentally upon photoirradiation for the ditopic compounds 10–12, TD-DFT modeling revealed absorbance maxima of 482 nm, 459 nm, and 502 nm for compounds 10, 11, and 12, respectively (Figures S93 and

S94). The trend was similar for all the targets (compounds 10-12), with an absorbance increase predicted going from the Z_iE isomers to the E_iE ones, accompanied by a red-shifted λ_{max} (Figures S93 and S94).

Concentration Dependent Studies. To assess the effect of $\pi - \pi$ interactions in solution on the extent of photoisomerization of these RCN oligothiophenes, concentrationdependent ¹H NMR studies (chloroform-d) were performed using 2-Z and 3-Z as model compounds (Figures S61 and S62). Samples of pure 2-Z were prepared in concentrations varying from 5 mM to 35 mM before each solution was irradiated to a PSS using blue LED light ($\lambda_{irr} = 454$ nm). The results of the experiment show a concentration dependence on the observed Z/E isomeric distributions at the PSS, ranging from 43/57 (2-Z/2-E) for the 5 mM sample to 60/40 (2-Z/2-E) for the 35 mM sample (Figure S61). The observed trends indicate that samples of higher concentration (35 mM) result in less $Z \to E$ conversion compared with more dilute samples (5 mM), possibly due to the greater extent of π - π interactions in solution for the more concentrated samples which may impede the degrees of freedom necessary to undergo isomerization reactions in solution.³² In addition, a gradual shielding effect was observed for the chemical shift of the 2-Z exocyclic olefin proton near 8.03 ppm, representing a chemical shift change from 8.031 ppm (5 mM) to 8.017 ppm (35 mM). The chemical shift values of other protons in the 2-Z/Emixture were also subject to change as a function of concentration (Figure S61). However, the exocyclic olefin protons corresponding to 2-Z (ca. 8.03 ppm) and 2-E (ca. 7.33 ppm) within the isomeric mixture underwent the most significant changes in chemical shift.

The concentration-dependent 1H NMR studies (chloroform-d) for compound 3 were performed using a concentration range from 1.25 mM to 30 mM upon irradiation to a PSS using 454 nm light (Figure S62). Similar to compound 2, the concentration of the samples is found to affect both the chemical shift and PSD in the case of 3-Z. Isomeric distributions ranging from 44/56 (3-Z/3-E) to 82/18 (3-Z/3-E) were observed upon irradiation of 1.25 mM and 30 mM samples of 3-Z, respectively. The observed discrepancies in Z/E isomeric distributions at the PSS indicate resistance toward Z \to E conversion for samples higher in concentration (Figure S62).

Comparing the concentration-dependent PSDs obtained for 3-Z with those observed for 2-Z, within a similar range of concentration of 5 mM-30 mM, it was determined that compound 3-Z experiences a greater degree of suppression of $Z \rightarrow E$ conversion at higher concentrations. This is reflected in the PSD range between 52/48 (3-Z/3-E) and 82/18 (3-Z/3-E) representing a 30% decrease in E isomer content as a function of increasing concentration from 5 mM to 30 mM (Figure 9, right spectra), whereas the PSDs for compound 2 range from 43/57 (2-Z/2-E) to 57/43 (2-Z/2-E), representing only a 14% decrease in $Z \rightarrow E$ conversion between 5 mM and 30 mM samples, respectively (Figure 9, left spectra). In addition, a gradual shielding effect was observed by ¹H NMR for the 3-Z exocyclic olefin proton, ranging from 8.032 to 8.015 ppm for the 5 mM and 30 mM samples, respectively (Figure 9, right spectra). The observed change in chemical shift $(\Delta \delta)$ was more pronounced for 3-Z $(\Delta \delta = 0.017 \text{ ppm})$ compared to 2-Z ($\Delta\delta$ = 0.011 ppm). The results of these experiments indicate that $\pi - \pi$ interactions are non-negligible for RCN-functionalized thiophenes in solution, and these



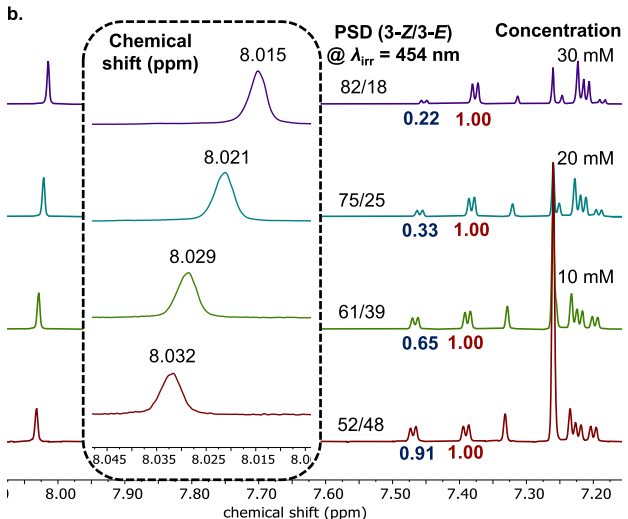


Figure 9. ¹H NMR spectra (chloroform-d) showing (a) 2-Z/2-E (top) and (b) 3-Z/3-E (bottom) isomeric distributions as a function of concentration increasing from 5 mM (bottom spectra) to 30 mM (top spectra). The change in chemical shift of the isomerizable olefin proton of the Z isomer is shown by the expanded inset (left).

interactions may be responsible for the observed changes in chemical shift and the varying Z/E isomeric distributions obtained at different solution concentrations.

The results observed for 2-Z and 3-Z may explain the lack of well-controlled Z/E isomerization observed for quarterthiophene RCN derivatives, compounds 4-Z and 9-Z, considering their larger extent of π conjugation and possibly stronger π - π interactions (Table 1). However, the associated energy change at the ground- and excited state levels upon increased conjugation³³ in compounds 4 and 9 might facilitate different photochemical pathways^{34,35} for these compounds leading to degradation over well-controlled photoisomerization. Although a significant effect of aggregation on the extent of photoisomerization is observed from the NMR studies (in the mM concentration range), almost no change in absorption profiles is recorded for compound 3-Z from 10-120 µM (Figure S96). Additionally, the $Z \to E$ photoisomerization is almost entirely inhibited for compound 4-Z even upon prolonged irradiation (24 h), as confirmed from the NMR study (15 mM, Figure S88). However, well-controlled $Z \rightarrow E$ photoisomerization is observed for 4-Z by UV-vis at 20 μ M, Figure S95) upon 454 nm light irradiation. This also highlights

that the quarterthiophenes might undergo aggregation at mM concentration restricting the photoisomerization process, unlike at μ M concentration. Considering this aggregation effect in solution and the significant impact of Z/E photoisomerization on thin-film morphology and optoelectronic properties observed in donor—acceptor oligothiophenes, ¹⁸ we believe the current structure—property analyses will broadly inform the OPV community to consider photoisomerization in the context of OPV applications.

UV–Vis Photoswitching Studies. Considering the well-behaved photoisomerization behavior of compounds 3-Z and 7-Z upon excitation using all visible light sources ($\lambda_{\rm irr}=454$, 523, and 628 nm), we studied the reversibility of the photoisomerization reactions by performing photoswitching studies with these compounds using alternating 454 and 628 nm irradiation (Figures S97 and S98). Compound 3-Z was irradiated in solution (20 μ M, chloroform) with a shorter wavelength light source ($\lambda_{\rm irr}=454$ nm) to promote $Z\to E$ isomerization to obtain a PSS, while exposing the PSS mixture to a longer wavelength of irradiation ($\lambda_{\rm irr}=628$ nm) promoted $E\to Z$ isomerization until a new PSS was reached (Figure 10

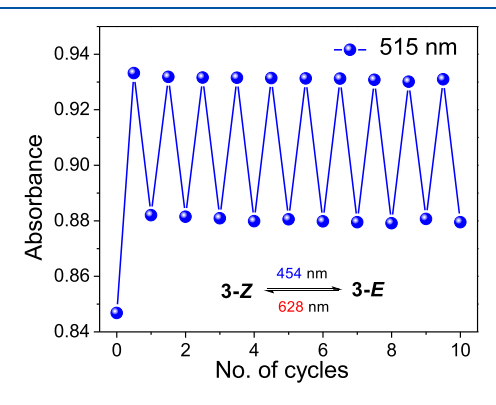


Figure 10. Photoswitching of compound 3-Z (chloroform, 20 μ M). The absorbance change at 515 nm was monitored while alternating between 454 and 628 nm wavelengths of irradiation.

and Figure S97). A similar photoswitching experiment was performed with compound 7-Z (Figure S98). Excitingly, even after ten photoswitching cycles, facile photoswitching was observed for both compounds with only minor evidence of photodegradation. The excellent fatigue-resistant behavior and facile photoswitching using visible light excitation bodes well for designing photoresponsive materials in the future.³⁶

Thermal Isomerization Studies. To investigate the thermal $E \rightarrow Z$ isomerization, a solution of compound 2-Z (15 mM, chloroform-d) was used considering its well-behaved photoisomerization behavior. A PSS mixture of 50/50 (2-Z/2-E) was kept in the dark and no thermal $E \rightarrow Z$ conversion was observed at room temperature (Figures S99 and S100). However, at an elevated temperature (40 °C), thermal isomerization was observed with the Z/E ratio obtained as 54/46 as monitored up to 120 h (Figure S101). To further investigate the solvent effect on thermal isomerization, samples of compound 2-Z were prepared in different polarity solvents, and thermal isomerization was monitored at 65 °C up to 24 h. The PSS ratio upon 454 nm irradiation of 2-Z/2-E was found to be 44/56, 50/50, and 41/59 in toluene- d_8 (Figure S104), tetrachloroethane-d₂ (Figure S106), and acetonitrile-d₃ (Figure S102), respectively, suggesting the extent of $Z \rightarrow E$ photoisomerization is dependent on the solvent medium. For

thermal $E \to Z$ isomerization, in less polar solvents like toluene- d_8 and tetrachloroethane- d_2 , only minor isomerization was observed, with the PSS ratio of 45/55 (Figure S105) and 52/48 (Figure S107), respectively. Interestingly, in a more polar solvent (acetonitrile- d_3), a PSS mixture of 41/59 (2-Z/2-E) was observed to revert to 70/30 (2-Z/2-E) at 65 °C to achieve thermal equilibrium (Figures S102 and S103). This observation of higher extent of thermal $E \to Z$ isomerization in a more polar solvent (e.g., 49% in acetonitrile) compared to less polar ones (e.g., 2% in toluene and 4% in tetrachloroethane) is consistent with our previous studies using INCN-functionalized thiophene photoswitches. ²⁷

NMR Photodegradation Studies. As a few RCNoligothiophene molecules did not undergo well-behaved photoisomerization, and resulted in photodegradation, more in-depth studies were performed using model compound 1-Z to investigate the fate of the molecule upon prolonged photoirradiation. In chloroform-d, as the irradiation time progresses, the disappearance of the isomerizable olefin proton (δ = 8.11 ppm) is observed, along with appearance of a singlet at $\delta = 5.39$ ppm, accompanied by other peaks that are inconsistent with 1-Z or 1-E structures (Figure S117). While the photoinduced side-product could not be confirmed from the preliminary NMR spectroscopic measurements (Figures S118 and S119), tandem pericyclic reactions or photoepoxidation reactions are suspected to occur, as reported for related INCN-functionalized thiophenes. ^{27,29,30} As both $Z \rightarrow E$ photoisomerization and $E \rightarrow Z$ thermal isomerization processes are found to be dependent on solvent medium, the photodegradation behavior was also tested in different polarity solvents. Both in toluene-d₈ (Figures S114-S116) and acetonitrile-d₃ (Figures S120-S122), a similar photochemical outcome was observed, with the disappearance of the olefin proton signal ($\delta_{\text{toluene-}d8} = 7.69$ ppm, and $\delta_{\text{acetonitrile-}d3} = 8.16$ ppm), accompanied by the appearance of a single peak $(\delta_{\text{toluene-}d8} = 5.53 \text{ ppm}, \text{ and } \delta_{\text{acetonitrile-}d3} = 5.40 \text{ ppm}). \text{ As the}$ photodegradation was monitored by the disappearance of the olefin proton peak, the photoinduced side reaction seems to be faster in a more polar solvent (within 24 h in acetonitrile- d_3 versus \sim 60 h in toluene- d_8 and chloroform-d). TLC analysis (in dichloromethane) revealed a similar R_f value for the side product as pure 1-Z (Figures S123-S125). Furthermore, the irradiated mixtures were passed through a silica column using dichloromethane as the eluent, where similar NMR spectra were obtained after purification for all three mixtures. This suggests the formation of similar photoproducts upon irradiation in all solvents (Figure S126). Direct analysis in real time (DART)-mass spectrometry (MS) confirms the same molecular mass for the photoirradiated products as compound 1-Z (molar mass: 371.517 g/mol, molecular formula: $C_{19}H_{21}N_3OS_2$), suggesting no reaction with exogenous species and eliminating photo-oxidation reactions (Figure S130-S133). More in-depth NMR spectroscopic analysis confirms a tandem pericyclic reaction is involved, where 1-Z can photoisomerize to 1-E, followed by consecutive 6π electrocyclic reaction and 1,5-sigmatropic rearrangement (Figure S127-S129). The aliphatic proton involved in the final 1,5-hydride shift step is found to be deshielded to 5.39 ppm, due to adjacent electronegative atoms, characteristic of the photocyclization process (Figure S128).

Theoretical Investigations. The ground-state configurational (Z and E) and conformational (s-trans and s-cis) preferences for compounds 1-Z-12-ZZ were investigated by

DFT at the B3LYP/6-31+G(d) level of theory as implemented in Gaussian 09.37 Monotopic RCN-functionalized target molecules (compounds 1-9) were optimized in the Z and Eisomeric forms at the two lowest energy conformations (s-cis and s-trans). The s-cis and s-trans conformers adopt a nearly planar geometry with respect to the adjacent rhodanine heterocycle and represent a 180° rotation about the σ bond connecting the first thiophene unit with the isomerizable exocyclic olefin between each planar conformation. The structures for each monofunctionalized RCN derivative are shown in the Supporting Information (Figures S108-S110). The ditopic RCN substrates (compounds 10, 11, and 12) were optimized in the Z_1Z and Z_2E olefin configurations, each adopting the two lowest energy conformational possibilities (scis and s-trans). While the E,E isomers were not observed experimentally for compounds 10-12, these structures were also modeled by DFT to simulate the ground-state frontier MO levels and relative energies. The line-angle structures for each difunctionalized target molecule are shown in the Supporting Information (Figures S111 and S112).

The structures of monotopic RCN target molecules varying in π -conjugation length (compounds 1–4) are shown in the Supporting Information (Figure S108), and the computationally derived data for these structures are summarized in Table S1. For compounds 1–4, the Z configurational isomer is found to be the global minimized structure. Both the Z and E configurational isomers adopt the s-trans conformation representing the lowest energy structures in their respective configurations, with their energy being lower relative to the corresponding s-cis conformers (Table S1). The detailed relative energy values of all possible conformers for compounds 1, 2, 3, and 4 are included in Table S1.

The structures of monotopic RCN target molecules bearing an extra solubilizing group on the thiophene adjacent to RCN (compounds 5-7) are shown in Figure S109, and the computationally derived data for these structures are summarized in Table S2. The configurational and conformational energetic trends for 5-7 match closely the trends observed for the targets 1-3. For compounds 5-7, the Z isomers in the s-trans conformation represent the lowest energy of all structures and are approximately 3.20-3.40 kcal mol^{-1} lower in energy than the corresponding E isomers in the s-trans conformation (Table S2). The monotopic RCN target molecules with aldehyde substitution (compounds 8 and 9, Figure S110) follow the previously established trends, wherein the Z isomers (in the s-trans conformation) are more stable than the corresponding E isomers by 3.20-3.33 kcal mol⁻¹ (Figure S110 and Table S3).

The stereochemical (Z and E) and conformational (s-cis and s-trans) possibilities for the difunctionalized RCN target molecules (compounds 10–12) are more complex given the di-RCN substitution. Each ditopic RCN target molecule can be optimized as the Z,Z isomer, the Z,E isomer, and the E,E isomer. Beyond stereochemical considerations for each RCN moiety, a ditopic substrate can adopt either an s-cis or s-trans conformation as the two lowest energy preferences, resulting in a total of 10 possible configurational/conformational combinations for each ditopic target molecule. The ditopic RCN substrates (compounds 10–12) were optimized in the Z,Z, Z,E, and E,E olefin configurations, each adopting the two lowest energy conformational possibilities (s-cis and s-trans). Each Z,Z isomer for compounds 10–12 were modeled in the s-trans/s-trans conformations (Figure S111a), s-trans/s-cis

conformations (Figure S111b), and s-cis/s-cis conformations (Figure S111c). The computationally derived data for the *Z*,*Z* configurations are summarized in Table S4. In general, the *Z*,*Z* (s-trans/s-trans) structures represent the global energy minimum for all three compounds compared to their other possible s-trans/s-cis or s-cis/s-cis conformers in the *Z*,*Z* configuration.

The Z,E isomeric structures for each difunctionalized target molecule are shown in Figure S108. For the Z,E isomers, there are four conformational possibilities associated with the ditopic RCN functionalization on each terminus of the respective thiophene π -systems. The possible structures include (Z)-s-trans/(E)-s-trans, (Z)-s-trans/(E)-s-cis, (Z)-s-cis/(E)-s-trans, and (Z)-s-cis/(E)-s-cis. The computationally derived data for compounds 10–12 in the Z,E configurations are summarized in Table S5. Similar to the trends observed previously with the Z,Z isomers, the Z,E isomers in the s-trans/s-trans conformations represent the lowest energy structures for all the ditopic compounds (Table S5).

The E,E isomeric structures for each difunctionalized target molecule are shown in Figure S113. Each E,E isomer for compounds 10-12 were modeled in the s-trans/s-trans conformations (Figure 113a), s-trans/s-cis conformations (Figure 113b), and s-cis/s-cis conformations (Figure 113c). The computationally derived data for the E_tE configurations are summarized in Table S6, which denotes that the s-trans/strans structure is the lowest energy conformation among the possible conformers adopting the E,E configuration. Comparing the lowest energy conformers (s-trans/s-trans) for all the possible different configurations (Z,Z; Z,E; and E,E) of the ditopic targets (10-12), the Z_1Z isomers (0.00 kcal/mol) are found to be the most stable compared to their Z_tE counterparts (2.93-3.20 kcal/mol), with the *E,E* ones being least stable (6.03-6.52 kcal/mol, Table S7). The high relative energy of the E₂E isomers at the ground-state might explain the fact that only $Z_{2}E$ isomers were obtained postirradiation of the $Z_{2}Z$ samples in solution, with no evidence of formation of the E,E isomers. A similar trend was observed for the fused bis(hemiindigo) derivatives of their energy-minimized ground- and excited-state structures.³⁸ Also acknowledging the fact that the electronic decoupling at the excited state has a significant impact on the photoisomerizable architectures consisting of multiple azo-bonds, 39,40 it would be beneficial to design novel difunctionalized RCN-oligothiophenes to achieve their E,E counterparts through structural modifications supported by indepth quantum chemical calculations in the future. This might be of more interest to the OPV community to investigate how the accumulation of the metastable E isomer of these RCNoligomers would affect the organic solar cell (OSC) efficiency.

CONCLUSIONS

An extensive structure—property relationship investigation has been performed with respect to the solution Z/E photoisomerization behavior of a library of monotopic (1-Z-9-Z) and ditopic (10-ZZ-12-ZZ) dicyanorhodanine (RCN)-functionalized thiophenes. The as-synthesized olefin stereochemistry for 1-Z-9-Z was determined to be the Z isomer in all cases, with the E form only obtained upon selective photoirradiation using UV ($\lambda_{\rm irr}=254$ nm) and visible ($\lambda_{\rm irr}=454,523$, and 628 nm) light. Stereochemical analysis of ditopic model compounds (10-ZZ-12-ZZ) has confirmed that the thermodynamically stable Z,Z isomers are obtained as the only detectable isomers from synthesis, whereas the Z,E forms were

formed upon irradiation to a photostationary state with no evidence of the corresponding E,E forms. An evaluation of the relative Z/E and Z,Z/Z,E gas-phase energies and conformational preferences via ground-state DFT calculations (B3LYP/6-31+G*) confirmed that the Z olefin stereochemistry in the strans conformation represents the lowest energy structural possibility for RCN units appended to all 12 target molecules.

The photoisomerization processes were monitored by NMR and UV-vis spectroscopic studies with good agreement. It was shown that all 12 RCN-functionalized thiophenes are susceptible to Z/E photoisomerization reactions in solution. For the monotopic target compounds, while alkylation at the thiophene unit shifted the absorption maximum to the red (\sim 20 nm) for monothiophene targets (1-Z and 5-Z), a ca. 4 nm blue-shift was observed for bis- (2-Z and 6-Z) and terthiophene (3-Z and 7-Z) compounds. A significant redshift was observed upon extending the π -conjugation with thiophene units, which also enable red-light-induced photoisomerization. Interestingly, quarterthiophene compounds 4-Z and 9-Z resist this process almost entirely except under ambient irradiation conditions. All the ditopic RCNoligothiophenes (10-ZZ-12-ZZ) were shown to undergo well-controlled photoisomerization upon visible-light irradiation, while extending the conjugation from bis- (10-ZZ) to terthiophene (10-ZZ) units suppressed $Z \rightarrow E$ isomerization. Importantly, concentration-dependent ¹H NMR photoisomerization studies revealed the role of aggregation for compounds 2-Z and 3-Z, where higher concentrations resulted in diminished $Z \rightarrow E$ conversion under 454 nm irradiation compared to more dilute samples in chloroform-d. The concentration-dependent chemical shift changes observed for the aromatic protons of 2 and 3 are consistent with $\pi-\pi$

Ending with a word of caution, all the studied RCN-oligothiophenes undergo well-behaved Z/E photoisomerization under ambient laboratory light conditions, yielding 6—26% of the metastable isomer. These percentages are more than sufficient to affect solid-state morphology and optoelectronic properties, and represent impurity levels well beyond the typical tolerances for OPV applications. We are hopeful that these in-depth structure—property investigations will continue to be of both practical importance to the organic optoelectronics community and inform the design of future generations of organic photoswitches.

EXPERIMENTAL METHODS

General Methods. Reagents and solvents were purchased from commercial sources and used without further purification unless otherwise specified. THF was degassed in a 20 L drum and passed through activated alumina under a positive argon atmosphere. Thinlayer chromatography (TLC) was performed on SiO₂-60 F₂₅₄ aluminum plates with visualization by UV light. Column chromatography was performed using silica gel technical grade, pore size 60 Å, 230-400 mesh particle size, 40-63 μ m particle size from Sigma-Aldrich. ¹H (¹³C) NMR were recorded on an INOVA-500 (¹H at 500 MHz; ^{13}C at 125 MHz) spectrometer and a Bruker 600 MHz spectrometer (1 H at 600 MHz; 13 C at 150 MHz). Chemical shifts (δ) are given in parts per million (ppm) referenced to residual deuterated solvent purchased from Cambridge Isotope Laboratories, Inc. (CDCl₃: δ H 7.26 ppm, δ C 77.16 ppm). Abbreviations used are s (singlet), d (doublet), t (triplet), q (quartet), quin (quintet), and m (multiplet). Electrospray ionization (ESI) high-resolution mass spectra (HRMS) were recorded on an Agilent 6210 TOF spectrometer with MassHunter software. Note: Due to the photosensitivity of the RCN-functionalized products, the reaction vessels

were covered with aluminum foil for the synthesis of 1-Z-12-ZZ. Aluminum foil was used to cover all glassware during purification processes such that any source of light exposure was eliminated while samples were dissolved in solution.

Computational Methods. Ground state geometries and conformational analyses were conducted in the gas phase at the B3LYP/6-31+G(d) level as implemented in Gaussian 09.³⁷ All octyl chains were truncated to methyl groups to reduce the computational cost. Excited-state calculations were performed at the CAM-B3LYP/cc-pVDZ level of theory using the coordinates from the previously optimized geometries. Molecular orbital plots were made using VMD from the Gaussian output files or using Avogadro visualization software. Frontier molecular orbitals were visualized using Avogadro molecular editor and visualization software.

UV–Vis Photoisomerization Experiments. Solution absorption spectra were measured for 20 μ M solutions of the compounds in chloroform on a PerkinElmer Lambda 25 dual beam absorption spectrometer and a Cary 100 Bio spectrophotometer using 1 cm quartz cells. Spectrophotometric grade solvents were used for the absorption studies. Solutions of 1-Z–12-ZZ (20 μ M in chloroform) were prepared and transferred into a quartz cuvette for immediate UV–vis absorption measurements. The solutions were then irradiated, and the UV–vis spectra were recorded to monitor the isomerization process. The photostationary states (PSS) were determined by continuous irradiation of the sample until no further changes in UV–vis spectra were observed. Note: For irradiation experiments requiring ultraviolet (254 nm) irradiation of RCN-thiophene solutions through a quartz medium, the quartz cuvette was placed inside a glass container before irradiation with ultraviolet light.

NMR Photoisomerization Experiments. ¹H NMR spectra were recorded on an INOVA-500 (¹H at 500 MHz) spectrometer. To determine the photostationary state composition of each RCN-functionalized target molecule, a 15 mM stock solution in chloroform-d was prepared. For ambient irradiation experiments, 7.5 mM solutions were used. Approximately 0.5 mL of the stock solution was placed in a conventional glass NMR tube unless otherwise specified. The samples were exposed to an appropriate irradiation wavelength and ¹H NMR spectra were recorded hourly. The integration ratios of signals corresponding to the Z isomer and the E isomer were compared to calculate a relative percentage of each species in solution. The samples were irradiated and ¹H NMR spectra were recorded until changes in the Z/E integration ratios were no longer observed, indicating that the photostationary state had been reached.

ASSOCIATED CONTENT

Data Availability Statement

The data underlying this study are available in the published article and its Supporting Information.

Supporting Information

The Supporting Information is available free of charge at https://pubs.acs.org/doi/10.1021/acs.joc.4c00823.

Synthesis, structural characterization details, computational data, isomerization experiments and associated NMR data, UV-vis isomerization data, irradiation sources, and computational details are provided in the Supporting Information (PDF)

AUTHOR INFORMATION

Corresponding Author

Ronald K. Castellano — Department of Chemistry, University of Florida, Gainesville, Florida 32611, United States;
orcid.org/0000-0003-4322-9932; Email: castellano@chem.ufl.edu

Authors

Cory T. Kornman – Department of Chemistry, University of Florida, Gainesville, Florida 32611, United States

Parag Das – Department of Chemistry, University of Florida, Gainesville, Florida 32611, United States

Lei Li – Department of Chemistry, University of Florida, Gainesville, Florida 32611, United States; Present Address: Department of Chemistry, Western Kentucky University, 1906 College Heights Blvd., Bowling Green, KY, 42101, USA; orcid.org/0000-0001-8901-4932

Asmerom O. Weldeab — Department of Chemistry, University of Florida, Gainesville, Florida 32611, United States;
orcid.org/0000-0002-3004-7841

Ion Ghiviriga — Department of Chemistry, University of Florida, Gainesville, Florida 32611, United States;
orcid.org/0000-0001-5812-5170

Complete contact information is available at: https://pubs.acs.org/10.1021/acs.joc.4c00823

Author Contributions

\$C.T.K. and P.D. contributed equally.

Funding

R.K.C. is thankful to the National Science Foundation for supporting this research (CHE-1904534; CHE-2203754). The mass spectrometric data were obtained by the UF Department of Chemistry Mass Spectrometry Research and Education Center supported, in part, by the National Institutes of Health (NIH S10OD021758-01A1 and S10 OD030250-01A1).

Notes

The authors declare no competing financial interest.

ACKNOWLEDGMENTS

Acknowledgment is made to National Science Foundation for funding this research (CHE-1904534; CHE-2203754). C. T. K. wishes to acknowledge the University of Florida (UF) Department of Chemistry for providing a Graduate School Fellowship (GSF) which made this research possible. We acknowledge the University of Florida Research Computing for providing computational resources and support that have contributed to the research results reported in this publication (https://www.rc.ufl.edu). The mass spectrometric data were obtained by the UF Department of Chemistry Mass Spectrometry Research and Education Center supported, in part, by the National Institutes of Health (NIH S10OD021758-01A1 and S10 OD030250-01A1). We would also like to thank the UF Center for Nuclear Magnetic Resonance Spectroscopy for providing equipment and support that have contributed to these published results.

■ REFERENCES

- (1) Behringer, H.; Falkenberg, K. Synthesen mit vinylogen Säurederivaten, VII. β . β -Substituierte 5-Äthyliden-rhodanine. *Chem. Ber.* **1966**, 99 (1), 307–313.
- (2) Long, G.; Wu, B.; Yang, X.; Kan, B.; Zhou, Y.-c.; Chen, L.-c.; Wan, X.; Zhang, H.-l.; Sum, T. C.; Chen, Y. Enhancement of Performance and Mechanism Studies of All-Solution Processed Small-Molecule based Solar Cells with an Inverted Structure. ACS Appl. Mater. Interfaces 2015, 7 (38), 21245–21253.
- (3) Insuasty, A.; Ortiz, A.; Tigreros, A.; Solarte, E.; Insuasty, B.; Martín, N. 2-(1,1-dicyanomethylene)rhodanine: A novel, efficient electron acceptor. *Dyes Pigm.* **2011**, *88* (3), 385–390.
- (4) Kan, B.; Li, M.; Zhang, Q.; Liu, F.; Wan, X.; Wang, Y.; Ni, W.; Long, G.; Yang, X.; Feng, H.; Zuo, Y.; Zhang, M.; Huang, F.; Cao, Y.; Russell, T. P.; Chen, Y. A Series of Simple Oligomer-like Small Molecules Based on Oligothiophenes for Solution-Processed Solar

- Cells with High Efficiency. J. Am. Chem. Soc. 2015, 137 (11), 3886–3893.
- (5) Sandoval-Torrientes, R.; Calbo, J.; García-Fresnadillo, D.; Santos, J.; Ortí, E.; Martín, N. Rhodanine-based dyes absorbing in the entire visible spectrum. *Org. Chem. Front.* **2017**, *4* (6), 1024–1028.
- (6) Privado, M.; de la Cruz, P.; Biswas, S.; Singhal, R.; Sharma, G. D.; Langa, F. A non-fullerene all small molecule solar cell constructed with a diketopyrrolopyrrole-based acceptor having a power conversion efficiency higher than 9% and an energy loss of 0.54 eV. *J. Mater. Chem. A* **2018**, *6* (25), 11714–11724.
- (7) Fan, Q.; Li, M.; Yang, P.; Liu, Y.; Xiao, M.; Wang, X.; Tan, H.; Wang, Y.; Yang, R.; Zhu, W. Acceptor-donor-acceptor small molecules containing benzo[1,2-b:4,5-b']dithiophene and rhodanine units for solution processed organic solar cells. *Dyes Pigm.* **2015**, *116*, 13–19.
- (8) Lu, B.; Zhang, Z.; Wang, J.; Cai, G.; Wang, J.; Yuan, X.; Ding, Y.; Wang, Y.; Yao, Y. Nonfullerene electron acceptors with electron-deficient units containing cyano groups for organic solar cells. *Mater. Chem. Front.* **2021**, *5* (15), 5549–5572.
- (9) Liu, H.; Li, Z. a.; Zhao, D. Rhodanine-based nonfullerene acceptors for organic solar cells. *Sci. China Mater.* **2019**, *62* (11), 1574–1596.
- (10) Duan, T.; Chen, Q.; Yang, Q.; Hu, D.; Cai, G.; Lu, X.; Lv, J.; Song, H.; Zhong, C.; Liu, F.; Yu, D.; Lu, S. Simple thiazole-centered oligothiophene donor enables 15.4% efficiency all small molecule organic solar cells. *J. Mater. Chem. A* **2022**, *10* (6), 3009–3017.
- (11) Zhang, Q.; Kan, B.; Liu, F.; Long, G.; Wan, X.; Chen, X.; Zuo, Y.; Ni, W.; Zhang, H.; Li, M.; Hu, Z.; Huang, F.; Cao, Y.; Liang, Z.; Zhang, M.; Russell, T. P.; Chen, Y. Small-molecule solar cells with efficiency over 9%. *Nat. Photonics* **2015**, 9 (1), 35–41.
- (12) Wang, H.; Zhao, C.; Burešová, Z.; Bureš, F.; Liu, J. Cyanocapped molecules: versatile organic materials. *J. Mater. Chem. A* **2023**, *11* (8), 3753–3770.
- (13) Morel, D. L.; Stogryn, E. L.; Ghosh, A. K.; Feng, T.; Purwin, P. E.; Shaw, R. F.; Fishman, C.; Bird, G. R.; Piechowski, A. P. Organic photovoltaic cells. Correlations between cell performance and molecular structure. *J. Phys. Chem.* **1984**, *88* (5), 923–933.
- (14) El-Zohry, A.; Orthaber, A.; Zietz, B. Isomerization and Aggregation of the Solar Cell Dye D149. *J. Phys. Chem. C* **2012**, 116 (50), 26144–26153.
- (15) El-Zohry, A. M.; Zietz, B. Concentration and Solvent Effects on the Excited State Dynamics of the Solar Cell Dye D149: The Special Role of Protons. *J. Phys. Chem. C* **2013**, *117* (13), 6544–6553.
- (16) Zietz, B.; Gabrielsson, E.; Johansson, V.; El-Zohry, A. M.; Sun, L.; Kloo, L. Photoisomerization of the cyanoacrylic acid acceptor group a potential problem for organic dyes in solar cells. *Phys. Chem. Chem. Phys.* **2014**, *16* (6), 2251–2255.
- (17) Kornman, C. T.; Li, L.; Weldeab, A. O.; Ghiviriga, I.; Abboud, K. A.; Castellano, R. K. Photoisomerization of dicyanorhodanine-functionalized thiophenes. *Chem. Sci.* **2020**, *11* (37), 10190–10197.
- (18) Camero, D. M.; Grinalds, N. J.; Kornman, C. T.; Barba, S.; Li, L.; Weldeab, A. O.; Castellano, R. K.; Xue, J. Thin-Film Morphology and Optical Properties of Photoisomerizable Donor—Acceptor Oligothiophenes. *ACS Appl. Mater. Interfaces* **2023**, *15* (21), 25134–25147.
- (19) Köttner, L.; Wolff, F.; Mayer, P.; Zanin, E.; Dube, H. Rhodanine-Based Chromophores: Fast Access to Capable Photoswitches and Application in Light-Induced Apoptosis. *J. Am. Chem. Soc.* **2024**, *146* (3), 1894–1903.
- (20) Das, P.; Grinalds, N. J.; Ghiviriga, I.; Abboud, K. A.; Dobrzycki, Ł.; Xue, J.; Castellano, R. K. Dicyanorhodanine-Pyrrole Conjugates for Visible Light-Driven Quantitative Photoswitching in Solution and the Solid State. J. Am. Chem. Soc. 2024, 146 (17), 11932–11943.
- (21) Gernet, A.; El Rhaz, A.; Jean, L. Easily Accessible Substituted Heterocyclic Hemithioindigos as Bistable Molecular Photoswitches. *Chem. Eur. J.* **2023**, 29 (48), No. e202301160.
- (22) Du, Z.; Chen, W.; Chen, Y.; Qiao, S.; Bao, X.; Wen, S.; Sun, M.; Han, L.; Yang, R. High efficiency solution-processed two-

- dimensional small molecule organic solar cells obtained via low-temperature thermal annealing. *J. Mater. Chem. A* **2014**, 2 (38), 15904–15911.
- (23) Weldeab, A. O.; Kornman, C. T.; Li, L.; Starkenburg, D. J.; Zhao, X.; Fagnani, D. E.; Sadovy, S. J.; Perry, S. S.; Xue, J.; Castellano, R. K. Structure—Assembly—Property Relationships of Simple Ditopic Hydrogen-Bonding-Capable π -Conjugated Oligomers. *Org. Mater.* **2021**, 3 (02), 390–404.
- (24) Norton Matos, M. R. P.; Gois, P. M. P.; Mata, M. L. E. N.; Cabrita, E. J.; Afonso, C. A. M. Studies on the Preparation of 4-Ethoxyalkyliden and 4-Aminoalkyliden-5(4H)-oxazolones. *Synth. Commun.* **2003**, 33 (8), 1285–1299.
- (25) Mrinalini, M.; Prasanthkumar, S. Recent Advances on Stimuli-Responsive Smart Materials and their Applications. *ChemPlusChem.* **2019**, *84* (8), 1103–1121.
- (26) Dong, H.; Zhu, H.; Meng, Q.; Gong, X.; Hu, W. Organic photoresponse materials and devices. *Chem. Soc. Rev.* **2012**, *41* (5), 1754–1808.
- (27) Das, P.; Kornman, C. T.; Ghiviriga, I.; Abboud, K. A.; Castellano, R. K. Enlightening the Well-Controlled Photochemical Behavior of 1,1-Dicyanomethylene-3-Indanone-Functionalized π -Conjugated Molecules. *Chem. Mater.* **2023**, 35 (19), 8122–8134.
- (28) Che, Y.; Niazi, M. R.; Izquierdo, R.; Perepichka, D. F. Mechanism of the Photodegradation of A-D-A Acceptors for Organic Photovoltaics**. *Angew. Chem., Int. Ed.* **2021**, 60 (47), 24833–24837. (29) Che, Y.; Niazi, M. R.; Chan, Q.; Ghamari, P.; Yu, T.; Ruchlin, C.; Yu, H.; Yan, H.; Ma, D.; Xiao, S. S.; Izquierdo, R.; Perepichka, D. F. Design of Furan-Based Acceptors for Organic Photovoltaics. *Angew. Chem., Int. Ed.* **2023**, 62, No. e202309003.
- (30) Liu, Z.-X.; Yu, Z.-P.; Shen, Z.; He, C.; Lau, T.-K.; Chen, Z.; Zhu, H.; Lu, X.; Xie, Z.; Chen, H.; Li, C.-Z. Molecular insights of exceptionally photostable electron acceptors for organic photovoltaics. *Nat. Commun.* **2021**, *12* (1), 3049.
- (31) Jin, X.; Li, S.; Guo, L.; Hua, J.; Qu, D.-H.; Su, J.; Zhang, Z.; Tian, H. Interplay of Steric Effects and Aromaticity Reversals to Expand the Structural/Electronic Responses of Dihydrophenazines. *J. Am. Chem. Soc.* **2022**, *144* (11), 4883–4896.
- (32) Lui, B. F.; Tierce, N. T.; Tong, F.; Sroda, M. M.; Lu, H.; de Alani, J. R.; Bardeen, C. J. Unusual concentration dependence of the photoisomerization reaction in donor—acceptor Stenhouse adducts. *Photochem. Photobiol. Sci.* **2019**, *18* (6), 1587—1595.
- (33) Milián-Medina, B.; Gierschner, J. π-Conjugation. WIREs Comput. Mol. Sci. 2012, 2 (4), 513–524.
- (34) Zimmerman, H. E. Some theoretical aspects of organic photochemistry. *Acc. Chem. Res.* **1982**, *15* (10), 312–317.
- (35) Dou, Y.; Allen, R. E. Detailed dynamics of a complex photochemical reaction: Cis—trans photoisomerization of stilbene. *J. Chem. Phys.* **2003**, *119* (20), 10658–10666.
- (36) Zhuang, Y.; Ren, X.; Che, X.; Liu, S.; Huang, W.; Zhao, Q. Organic photoresponsive materials for information storage: a review. *Adv. Photonics* **2021**, *3* (1), No. 014001.
- (37) Frisch, M. J.; Trucks, G. W.; Schlegel, H. B.; Scuseria, G. E.; Robb, M. A.; Cheeseman, J. R.; Scalmani, G.; Barone, V.; Mennucci, B.; Petersson, G. A.; Nakatsuji, H.; Caricato, M.; Li, X.; Hratchian, H. P.; Izmaylov, A. F.; Bloino, J.; Zheng, G.; Sonnenberg, J. L.; Hada, M.; Ehara, M.; Toyota, K.; Fukuda, R.; Hasegawa, J.; Ishida, M.; Nakajima, T.; Honda, Y.; Kitao, O.; Nakai, H.; Vreven, T.; Montgomery, J. A., Jr.; Peralta, J. E.; Ogliaro, F.; Bearpark, M.; Heyd, J. J.; Brothers, E.; Kudin, K. N.; Staroverov, V. N.; Keith, T.; Kobayashi, R.; Normand, J.; Raghavachari, K.; Rendell, A.; Burant, J. C.; Iyengar, S. S.; Tomasi, J.; Cossi, M.; Rega, N.; Millam, J. M.; Klene, M.; Knox, J. E.; Cross, J. B.; Bakken, V.; Adamo, C.; Jaramillo, J.; Gomperts, R.; Stratmann, R. E.; Yazyev, O.; Austin, A. J.; Cammi, R.; Pomelli, C.; Ochterski, J. W.; Martin, R. L.; Morokuma, K.; Zakrzewski, V. G.; Voth, G. A.; Salvador, P.; Dannenberg, J. J.; Dapprich, S.; Daniels, A. D.; Farkas, O.; Foresman, J. B.; Ortiz, J. V.; Cioslowski, J., Fox, D. J. Gaussian 09, Revision D.01, Gaussian, Inc.: Wallingford CT, 2013.

- (38) Berdnikova, D. V.; Kriesche, B. M.; Paululat, T.; Hofer, T. S. Fused Bis(hemi-indigo): Broad-Range Wavelength-Independent Photoswitches. *Chem. Eur. J.* **2022**, 28 (71), No. e202202752.
- (39) Cisnetti, F.; Ballardini, R.; Credi, A.; Gandolfi, M. T.; Masiero, S.; Negri, F.; Pieraccini, S.; Spada, G. P. Photochemical and Electronic Properties of Conjugated Bis(azo) Compounds: An Experimental and Computational Study. *Chem. Eur. J.* **2004**, *10* (8), 2011–2021.
- (40) Bléger, D.; Dokić, J.; Peters, M. V.; Grubert, L.; Saalfrank, P.; Hecht, S. Electronic Decoupling Approach to Quantitative Photoswitching in Linear Multiazobenzene Architectures. *J. Phys. Chem. B* **2011**, *115* (33), 9930–9940.

